Eur. J. Mech. B - Fluids 19 (2000) 615–636

S0997-7546(00)00126-6/FLA

An experimental study of oblique transition in a Blasius boundary layer flow

Per A. Elofsson, P. Henrik Alfredsson *

Department of Mechanics, KTH, S-100 44 Stockholm, Sweden

(Received 27 April 1999; revised and accepted 7 March 2000)

Abstract – Transition initiated by a pair of oblique waves was investigated experimentally in a Blasius boundary layer flow by using hot-wire measurements and flow visualisation. The oblique waves were generated by periodic blowing and suction through an array of pipes connecting to the flow through a transverse slit in the flat plate model. The structure of the flow field is described and the amplitude of individual frequency-spanwise wave number modes was determined from Fourier transforms of the disturbance velocity. In contrast to results from investigations of oblique transition at subcritical flow conditions, the transition process at the present conditions suggests the combined effect of non-modal growth of streaks and a second stage with exponential growth of oblique waves to initiate the final breakdown stage. © 2000 Éditions scientifiques et médicales Elsevier SAS

oblique transition / boundary layer flow / non-modal disturbance

1. Introduction

The importance of three-dimensional disturbances in the transition process has been recognized since the boundary layer measurements by Klebanoff, Tidstrom and Sargent [1], who found it necessary to control the three-dimensionality in their experiments by placing strips of tape below the vibrating ribbon used for generating wave disturbances. The secondary instability scenario considers initially two-dimensional (Tollmien–Schlichting or TS) waves which grow in amplitude and develop into a three-dimensional stage. Two different three-dimensional stages have been identified, one in which Λ-shaped structures appear in an aligned pattern and another stage where Λ-shaped structures are seen in a staggered pattern. Transition involving the former is usually denoted K-type (after the first investigation by Klebanoff et al. [1]) or fundamental transition, whereas the staggered structures are part of the transition scenario denoted H-type, N-type or subharmonic. The first experimental observation of subharmonic transition was made by Kachanov, Kozlov and Levchenko [2] and the transition scenario has later been carefully investigated by, e.g., Corke and Mangano [3] with the use of controlled two- and three-dimensional waves.

The secondary instability theory was put forward by Orszag and Patera [4] and Herbert [5]. Further information on the concept of secondary instability can be found in the review by Herbert [6]. Experimental studies on the breakdown mechanisms of boundary layer flows are described by Kachanov [7] and information on numerical investigations is presented in the review by Kleiser and Zang [8].

Results both from experiments with forced TS-waves and Direct Numerical Simulations (DNS) have indeed been in close agreement with the secondary instability theory. In this study we use wave disturbances to study a different type of breakdown, as compared to the standard TS-wave scenario, by using two interacting oblique waves of small amplitude. This is the so-called oblique transition scenario (see Schmid and Henningson [9]). It is important to recognize that once the amplitude of the oblique waves in the subharmonic transition

* Correspondence and reprints; e-mail: hal@mech.kth.se

scenario becomes large, similar conditions exist as for the initial stage in oblique transition and the downstream development may therefore have some similarities. On the other hand the initial growth of streaky structures in the oblique transition scenario resembles some types of by-pass transition, as, for instance, the transition induced by free stream turbulence. It is therefore also a suitable way to model this type of by-pass transition through well described initial conditions.

1.1. Oblique transition

Oblique transition originates from the nonlinear interaction between a pair of oblique waves with wave angles of equal magnitude but opposite sign. Nonlinear interaction distributes disturbance energy among various wave numbers, and in particular to small streamwise wave numbers which can experience a strong non-modal growth (sometimes called 'transient growth'). If the amplitude of the streamwise streaks reaches above a threshold the streaks may become unstable with respect to low amplitude time-dependent disturbances and the flow may break down. Non-modal growth is operative also at low Reynolds numbers, and this implies that transition can occur at subcritical Re.

The first study of oblique transition in an incompressible flow was the direct numerical simulations by Schmid and Henningson [9]. They used a pair of finite amplitude oblique waves as initial conditions in temporal simulations of transition in plane Poiseuille flow at subcritical Reynolds numbers. The use of oblique waves resulted in a rapid growth of disturbance energy followed by breakdown. This growth was identified as resulting from a linear mechanism and the dominating structure was a streamwise independent structure with twice the spanwise wavenumber of the original oblique waves. When compared with the traditional secondary instability scenario starting with similar initial disturbance energy, oblique transition was found to be considerably faster.

Other investigations of oblique transition are the calculations using PSE (Parabolic Stability Equations) theory and spatial DNS by Joslin, Streett and Chang [10] and the spatial DNS by Berlin, Lundbladh and Henningson [11]. Both of these studies dealt with oblique transition in a boundary layer flow at zero pressure gradient. Joslin et al. did not reach a fully developed turbulent stage despite a longer computational box and a higher Re at the inflow. It was suggested that the reason for this was a difference in inflow conditions. Berlin et al. used Orr–Sommerfeld modes where the normal vorticity was excluded whereas Joslin et al. made use of complete eigenmodes.

In the study by Berlin et al. [11] it was conjectured that oblique transition in shear flows involves three stages. Firstly, a nonlinear generation of streamwise vortices by the oblique waves; secondly, generation of streaks through the 'lift-up' effect; and thirdly, breakdown due to a secondary instability operating on the streaks.

Elofsson and Alfredsson [12,13] made experiments on oblique transition in plane Poiseuille flow, where the pair of waves were generated by two vibrating ribbons mounted at opposite channel walls. For initial wave amplitudes in a lower range, elongated streamwise structures slowly decayed after an initial growth. For higher wave amplitudes, disturbances with a fundamental or superharmonic frequency to the initial waves increased in amplitude and breakdown eventually occurred. The experimental findings confirmed the results from the previous numerical simulations.

An experimental investigation of oblique transition in a flat plate boundary layer was carried out at DLR in Göttingen by Wiegel [14]. He used particle image velocimetry (PIV) and hot-wire anemometry to document the flow field obtained by controlled forcing with a wave generator using blowing and suction. These measurements showed the flow structure and provided information about the growth in streak amplitude and u_{rms} in various frequency bands. A comparison between the measurements of Wiegel and direct numerical simulations was made by Berlin, Wiegel and Henningson [15]. The closest agreement was obtained when the experimental wave generator was modelled in detail by prescribing the boundary conditions for the wall-

normal disturbance velocity at the wall in a step-wise fashion, and by using different amplitudes for positive and negative disturbance velocity. By imposing a pressure gradient in the simulations, the initial agreement with the experimental data was further improved. Berlin et al. also described the similarities between oblique transition and the two transition scenarios that are described with the secondary instability theory (K- and N-type transition).

The importance of a pair of oblique waves has also been recognized in other flow situations, thus indicating a generality of the transition scenario. For a flat plate boundary layer at low supersonic Mach numbers, the most unstable modes are oblique. This fact makes the oblique transition concept perhaps even more interesting in compressible flows. Fasel, Thumm and Bestek [16] investigated two different transition scenarios in a compressible boundary layer at a Mach number of 1.6 with the aid of direct numerical simulations. Despite a lower initial amplitude, the simulation with a pair of oblique waves as boundary conditions resulted in much faster breakdown than for their simulation of fundamental transition (i.e. transition initiated by a two-dimensional wave and a pair of oblique waves with a fundamental frequency). Similar results were obtained by Chang and Malik [17] who used nonlinear PSE calculations to compare oblique and subharmonic transition at a Mach number of 1.6. They found that transition originating from a pair of oblique waves required lower initial amplitudes than for the secondary instability of subharmonic type.

Other studies of oblique transition are those of Gathmann, Si-Ameur and Mathey [18] in a supersonic shear layer and Sandham, Adams and Kleiser [19] in a compressible flat plate boundary layer at a Mach number of 2.

1.2. Non-modal growth

The second stage in the oblique transition scenario is the generation and non-modal growth of streaks, where the growth results from an inviscid algebraic instability (see Ellingsen and Palm [20] and Landahl [21]).

One of the first studies which showed the existence of non-modal growth in a viscous flow was the work by Hultgren and Gustavsson [22]. They investigated the temporal development of three-dimensional disturbances in a parallel boundary layer flow and found an initial linear growth followed by a viscous decay. Later investigations have been able to quantify the growth in different flow situations and also to determine the optimal disturbance type. Some examples of such studies are Boberg and Brosa [23], Gustavsson [24], Butler and Farrell [25], Klingmann [26] and Trefethen et al. [27]. For further references see the review by Henningson [28].

Recent work on the spatial instability in Blasius flows have shown that the largest spatial energy growth occurs for streamwise vortices near the leading edge which evolves into streamwise streaks further downstream. Luchini [29] used a Reynolds number independent formulation and found that the maximum spatial growth occurred for vortices with a spanwise wavenumber of $\beta\delta = 0.45$ ($\beta = 2\pi/\lambda_z$ where λ_z is the spanwise wavelength and $\delta = \sqrt{\nu x/U_0}$). The same value of the optimal spanwise wavenumber was also found by Andersson, Berggren and Henningson [30] for $Re_x = 10^6$ and larger. In addition to these results they also proposed a simple model for prediction of the transition location. The model involved a single constant which was found to correlate well with experimental data on transition at free stream turbulence levels ranging from 1% to 5%.

1.3. Breakdown of streaks

During the last stage in the oblique transition scenario the streaks break down due to a secondary instability. For streaks initiated either by streamwise vortices directly or by vortices generated from a pair of oblique waves,

Reddy et al. [31] found that the threshold energy for transition in channel flows through streak breakdown is at least two orders of magnitude lower than for transition initiated by TS-waves at subcritical Reynolds numbers.

An experimental work by Elofsson, Kawakami and Alfredsson [32] on streak instability in plane Poiseuille flow showed that growth rates for the secondary instability increased linearly with the streak amplitude and that the most unstable mode was sinuous (or anti-symmetric). The streaks were generated by continuous suction and the secondary instability was studied by using controlled forcing from an earphone or a pair of earphones.

It can be noticed that since the range of amplified frequencies is rather wide, the frequencies seen in the breakdown stage of oblique transition will rather be the harmonics of the initial waves which are in the amplified range and not the specific frequency which experiences the largest growth. This is in contrast to the situation where streak breakdown is initiated by random background disturbances.

In the work by Waleffe [33,34], streak breakdown was identified as one element in a self-sustaining process for shear flow instability. Waleffe also hypothesized that this process occurs in the near-wall region of turbulent shear flows.

Bakchinov et al. [35] observed streak breakdown in an experimental work in a Blasius boundary layer flow. Streamwise vortices were generated by elongated roughness elements and the breakdown of the streaks were investigated both at unforced conditions and for the case with controlled excitation of wave disturbances by a vibrating ribbon. The instability of the spanwise modulated mean flow was found to be similar to the sinuous mode observed in Görtler flows.

The experimental setup is described in section 2 with special emphasis on the method used for generating the wave disturbances. In section 3 the flow quality is adressed, both by describing the characteristics of the mean flow and by comparing experimental results for single waves with stability theory. Experimental results on oblique transition are presented in section 4, and section 5 contains some further discussion and concluding remarks.

2. Experimental arrangement

The measurements were made in the MTL wind tunnel at the Department of Mechanics, KTH. This is a closed return tunnel with a streamwise turbulence intensity in the empty test-section of less than 0.02% in the velocity range $10 - 60$ m/s (see Johansson [36]). A flat plate model was installed horizontally in the 7 m long test section (cross section 0.8 by 1.2 m^2). The model is equipped with a trailing edge flap and has an asymmetric leading edge which results in a short pressure gradient region at the leading edge. A fine-meshed screen was installed 50 mm upstream of the hinge for the trailing edge flap. The combination of the screen and the flap was used to adjust the flow at the leading edge to compensate for the extra blockage below the plate due to the pipes and tubes for the disturbance generation, (without the screen a flap angle of about 11° would have been required). The experimental setup is shown in *figure 1(a)*.

A co-ordinate system is used with the x-axis in the streamwise direction, the y-axis is normal to the flat plate and the z-axis is in the spanwise direction. The origin is located on the centreline at the leading edge and the y-position is the distance from the surface of the plate. The velocities associated with the (x, y, z) co-ordinate system are (u, v, w).

The streamwise velocity component was measured with 2.5 μm platinum single wire probes using an AN-1003 constant temperature anemometer. The variation in the wind tunnel air temperature during measurements was within $\pm 0.1°$ and no temperature corrections of the anemometer signal was therefore deemed necessary. The hot-wire probe was positioned with a 5-axis traversing system controlled by a Macintosh Q950. This computer also controlled the National Instruments cards that were used for data acquisition and waveform

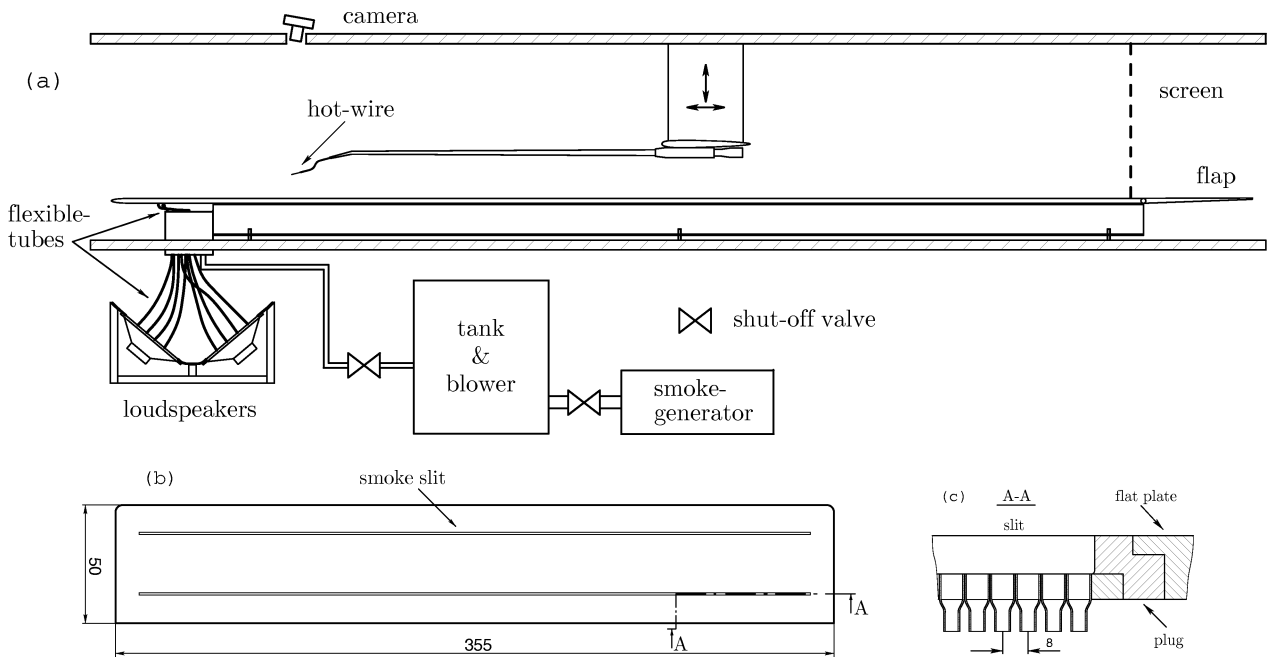

Figure 1. Experimental arrangement: (a) side-view of part of the test section with external equipment; (b) plug containing smoke slit and disturbance source; (c) cut-view. All measurements in millimeters.

generation. In order to avoid aliasing problems, the hot-wire signal was low-pass filtered before it was acquired with a 16-bit A–D converter. Two different methods were used during the measurement sessions, either the filter built into the anemometer or an external programmable filter with a linear phase (Kemo VBF10).

For the flow visualisation studies, a thin sheet metal was placed on top of the flat plate model in the region downstream of the disturbance source. The sheet metal (with a thickness of 0.5 mm) was painted black and its upstream end was chamfered to give a smooth junction to the surface of the flat plate model. A homogeneous smoke layer was introduced inside the boundary layer through a transverse slit located 212 mm downstream of the leading edge. The smoke produced by a fog-generator entered a tank which was connected to the smoke slit in the flat plate. To control the thickness of the smoke layer, the tank was equipped with a variable pressure blower and a valve at the outlet. Optical access for the camera was through a hole in the ceiling of the wind tunnel and light was provided by a flashlight mounted downstream the camera but inside the test section.

2.1. Generation of wave disturbances

Controlled wave disturbances are generated through a transverse slit located 189 mm downstream the leading edge. The slit has a spanwise length of 330 mm, a streamwise width of 0.8 mm and is 10 mm deep. An insert, consisting of 40 pipes equidistantly spaced in the spanwise direction, is mounted below the slit. The pipe outlets that face the bottom of the slit have been flattened to give a rectangular cross section and the other end of the pipes are connected to loudspeakers (diameter = 254 mm, 100 W) with flexible tubes. Details of the disturbance source are shown in *figure 1* together with an overview of the experimental setup. Inserts with different cross sections and spanwise spacing were manufactured; however the measurements reported were made with a pipe cross section of 0.8 mm by 6.0 mm and a spanwise spacing of 8.0 mm, unless otherwise stated. By changing the loudspeaker signals and the connection pattern of the tubes, it was possible to generate two-dimensional

Table I. Forcing signals for one wavelength at $\Delta\varphi = 60°$.

Pipe no.	$n=0$	1	2	3	4	5
Pair of waves	$2\sin(\omega t)$	$\sin(\omega t)$	$-\sin(\omega t)$	$-2\sin(\omega t)$	$-\sin(\omega t)$	$\sin(\omega t)$
Single wave	$\sin(\omega t+\frac{n\pi}{3})$					

and/or oblique waves and also to control the spanwise wavelength (in discrete steps) of the oblique waves. The method used for disturbance generation is similar to the one reported by Bake, Kachanov and Fernholz [37] and originally described by Gaponenko and Kachanov [38].

At maximum six loudspeakers were used in the present measurements. The signals for the loudspeakers were generated with a 6 channel D–A board and audio amplifiers were used for driving the loudspeakers. A connector box equipped with precision potentiometers allowed fine adjustment of the amplitude of separate loudspeakers. Each loudspeaker was fitted with a cover plate from which flexible tubes connected to the pipes of the disturbance source.

The experiments were focused on measurements of transition initiated by a pair of oblique waves with equal streamwise wavenumbers and spanwise wavenumbers of equal magnitude but opposite sign. In addition to the studies of oblique transition initial measurements were also made on single oblique waves.

A single oblique wave is obtained if the following signal is used for the loudspeaker driving the pipe with index n

$$A_n = A\sin(\omega t + n\Delta\varphi),$$

where A is the amplitude, ω is the angular frequency and $\Delta\varphi$ is the phase shift between consecutive pipes. Using the same notation, the loudspeaker signal required when generating a pair of oblique waves can be written as

$$\begin{aligned} A_n &= A\sin(\omega t + n\Delta\varphi) + A\sin(\omega t - n\Delta\varphi) \\ &= 2A\sin(\omega t)\cos(n\Delta\varphi). \end{aligned}$$

As an example *table I* compares the signals required for a single wave and for a pair of waves when the phase shift between individual pipes is 60°. This case corresponds to the conditions used for most of the measurements and it results in a spanwise wavelength of 48 mm. From the table it can be seen that for the generation of a single oblique wave six different signals are needed for each spanwise wavelength, whereas only four unique signals are required when a pair of oblique waves are being forced.

The loudspeaker voltages were carefully adjusted at a reference level. Since the loudspeakers were operated in their linear range, different wave amplitudes could easily be generated by adjusting the speaker voltages to values obtained by multiplying all the reference voltages by the same factor. The spanwise uniformity in wave amplitude was always better than 1%, whereas the variation in phase across the span was less than 0.4°. Note that for the case with a pair of oblique waves, the uniformity in amplitude applies to the amplitude at peaks and the uniformity in phase is within the regions between the 180° phase shifts.

2.2. Experimental conditions and procedure

Most of the measurements were made with free stream velocities of $U_0 = 8.2$ m/s or 9.1 m/s. Initial measurements with a single oblique wave were also made at lower velocities and the flow visualisations were made for velocities ranging from about 4 m/s up to 10 m/s. Wave frequencies range from $f = 38$ Hz to $f = 80$ Hz and they are usually expressed as the non-dimensional frequency parameter ($F = 2\pi f\nu \cdot 10^6/U_0^2$).

Measurements of length are expressed in millimeters in horizontal planes whereas wall-normal distances are either given in mm or as the non-dimensional Blasius co-ordinate ($\eta = y\sqrt{U_0/\nu x}$).

To describe the measurement results we decompose the velocity field $U(x, y, z, t)$ in a time averaged $\overline{U}$ and a fluctuating part u,

$$U(x, y, z, t) = \overline{U(x, y, z)} + u(x, y, z, t). \tag{1}$$

As a measure of the strength of the stationary disturbance field we use U_d defined as

$$U_d(x, y, z) = \overline{U(x, y, z)} - \frac{1}{z_1 - z_0} \int_{z_0}^{z_1} \overline{U(x, y, z)}\, \mathrm{d}z, \tag{2}$$

where z_0 and z_1 are the spanwise limits of the measurement region. For the fluctuating disturbance field we either use the amplitude (half the peak-to-peak value) or the root mean square of the streamwise disturbance velocity. These measures are denoted u' and u_{rms}, respectively. The notation u' is connected to a single frequency component (usually the generated frequency), whereas u_{rms} is the sum over all frequencies unless a specific frequency is stated, $u_{rms,f}$.

The structure of the flow was mapped out by traversing the hot-wire probe and measuring sets of data triggered by a reference signal from the waveform generation. Data was obtained in the following ways: by measuring wall-normal profiles at a fixed spanwise location for various streamwise positions (xy-plane); by traversing the probe in the spanwise direction at a fixed η for various streamwise positions (xz-plane); and by measurements of wall-normal profiles at a fixed streamwise location for various spanwise positions (yz-plane). In addition to these measurements in complete planes, numerous profiles were measured at single locations. Besides the measurements of the perturbed flow, wall-normal profiles were also measured at fully laminar (unperturbed) conditions. These profiles were used for obtaining the wall-normal position.

Each measurement position typically involved 20 triggered sets of 4096 points acquired with a sampling frequency in the range between 3.5 kHz and 5 kHz. The frequency was adjusted so that each set contained an integer number of periods of the generated wave. The laminar measurements involved fewer (untriggered) samples acquired with a lower frequency.

3. Flow quality

Information about the flow quality in the setup is presented by showing the pressure distribution along the flat plate model and also by comparing measurements for a single oblique wave with results from stability calculations.

Figure 2 shows the pressure distributions above the plate, obtained from hot-wire measurements outside the boundary layer edge and then calculated as $c_p = 1 - (u/u_{ref})^2$. Local peaks are observed in the streamwise distribution of c_p near $x = 120$ and $x = 160$ mm. The former is probably caused by a sealed slit at $x = 95$ mm, which was used in a previous experiment, whereas the latter peak is at the leading edge junction. The spanwise distribution at $x = 120$ mm shows a minimum at $z = 0$ and an increasing value of c_p to the sides. This is probably a result of the blockage from the tubes of the disturbance source, which extend ≈ 20 mm below the plate at a position of 190 mm from the leading edge. However, this effect is not observed in the measurements at $x = 500$ mm.

The variation in the shape factor (H_{12}) was found to be within $\pm 0.5\%$ from measurements, on several occasions, at five spanwise positions over a region of $z = \pm 150$ mm for every 100 mm in the streamwise

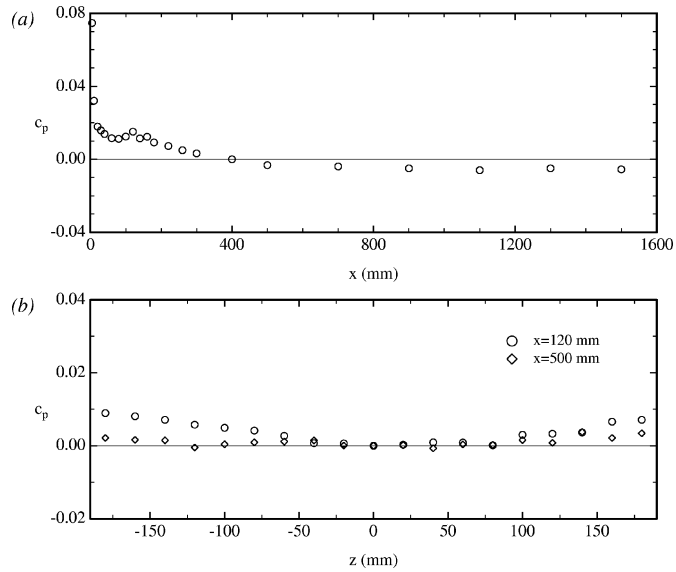

Figure 2. Pressure distribution obtained from hot-wire measurements for $U_0 = 7.0$ m/s: (a) Streamwise distribution, reference position is at $x = 400$ mm; (b) spanwise distributions at $x = 120$ and 500 mm.

direction. However, the mean value was $H_{12} = 2.63$ which is slightly above the theoretical value for a Blasius boundary layer. The reason for this deviation is not clear, but may be due to an inaccuracy in the determination of the $y = 0$ position.

3.1. Comparison with stability theory

In order to verify the quality of the disturbance source, measurements were also made when a single oblique wave was generated and the results were compared with PSE calculations.

Figure 3 shows wall-normal profiles of amplitude and phase at the frequency of the generated oblique wave. Results from measurements with $U_0 = 8.2$ m/s and $F = 106$ at three different streamwise positions are compared with stability theory. The amplitudes have been normalised with their maximum (the largest amplitude from the measurements was $u' = 1.0\%$ at $x = 210$ mm) and the phase profiles were uniformly shifted to match in the outer part of the boundary layer. Both the amplitude and the phase profiles are in agreement with theoretical distributions at $x = 510$ mm, but the deviation between measurements and PSE calculations is larger closer to the disturbance source. One can note that the first amplitude and phase profiles were measured at a position located only 20 mm downstream of the slit. This distance should be related to the streamwise wavelength at these conditions which is ≈ 41 mm.

The streamwise evolution of the maximum of a measured amplitude is compared with PSE results in *figure 4*. These experimental data were obtained by traversing the hot-wire probe through the amplitude maximum at conditions for which $U_0 = 8.2$ m/s and $F = 59$. Streamwise coordinates are expressed as $\sqrt{Re_x}$ and the amplitude from measurements and calculations have been normalised with their respective values at the first measurement position ($\sqrt{Re_x} = 330$). The measured amplitude maximum initially decays less than the calculated, but downstream of $\sqrt{Re_x} = 400$ the measurements indicate a lower amplitude. One explanation for the deviation between measurements and theory may be the relatively high initial amplitude, which is required if one should be able to measure the amplitude downstream at these damped conditions. The maximum amplitude at the first streamwise position was $u' \approx 1.6\%$.

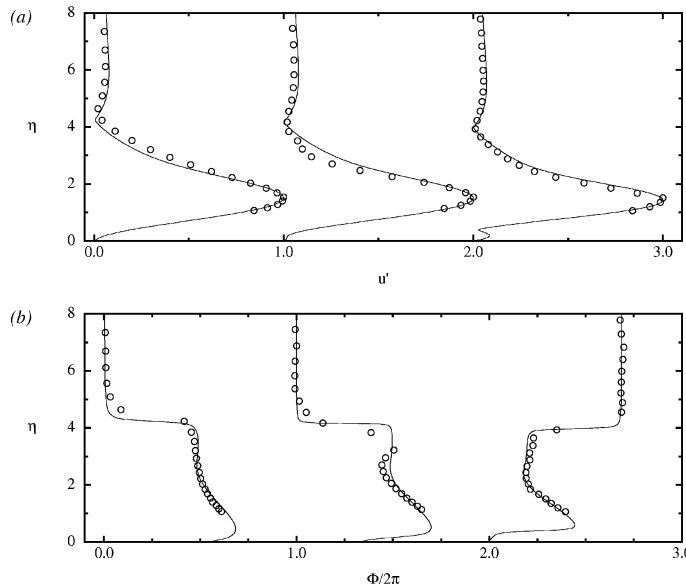

Figure 3. Comparison between: ○, measurements; ——, PSE calculations by A. Hanifi: (a) Amplitude profiles at $x = 210$, 270 and 510 mm; (b) corresponding phase profiles. $F = 106$, $U_0 = 8.2$ m/s and $\beta = 131$ m^{-1}.

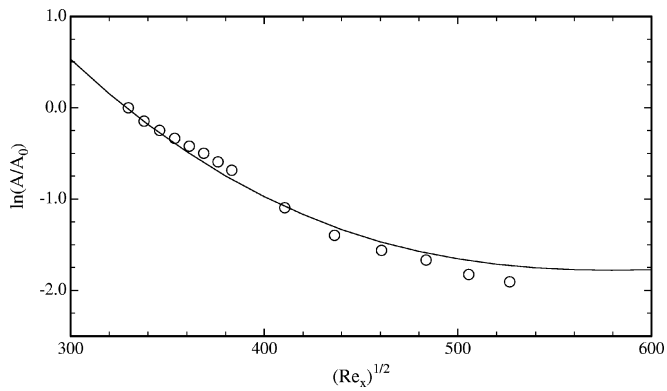

Figure 4. Amplitude evolution: ○, measurements; ——, PSE calculation by A. Hanifi. $F = 59$, $U_0 = 8.2$ m/s and $\beta = 131$ m^{-1}.

Another aspect which is important to consider when evaluating the quality of a disturbance generator is the spanwise uniformity of the generated waves. With the technique used in the present experiment, the spanwise uniformity is mainly governed by the similarity of the individual pipes and how the loudspeaker amplitudes have been adjusted. For the test measurements with a single oblique wave, one iteration with adjustments of the loudspeaker amplitudes was usually considered sufficient. The uniformity obtained after such a coarse adjustment is shown in *figure 5*. This figure shows the spanwise distribution of wave amplitude and phase obtained by traversing the hot-wire probe at a constant height 20 mm downstream of the wave generator. The deviation from the average wave amplitude is within 9 % at this streamwise position, however, further away from the disturbance source the uniformity is improved.

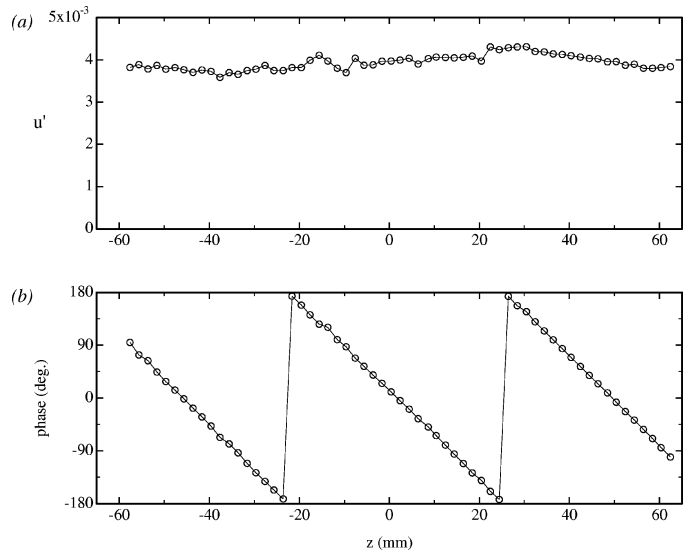

Figure 5. Oblique wave at $F = 200$, $U_0 = 6.0\,\mathrm{m/s}$ and $\beta = 131\,\mathrm{m}^{-1}$: (a) Spanwise profile of amplitude; (b) corresponding phase profile. Measurements at $x = 210$ mm near $\eta = 1.5$.

4. Oblique transition results

4.1. Flow structure

A dominating feature of the oblique transition scenario is the formation of large amplitude longitudinal structures.

The photo in *figure 6* shows a top view of the flow. A dimensional forcing frequency of $f = 51$ Hz was used and the velocity is $U_0 = 7.0$ m/s giving $F = 97$. The photo displays a streamwise length of 422 mm starting 40 mm downstream of the slit from which the disturbances are generated. The spanwise distance is 229 mm at the upstream side of the photo (the flow is from left to right in the figures) and 206 mm at the downstream end. For constant free stream and forcing conditions, the breakdown position can be altered by changing the amount of smoke seeped into the boundary layer. This was utilized in the figure to allow the whole transition scenario to be observed at one camera position. A wave field is observed in the left part of the photo and further downstream Λ-shaped structures appear in a staggered pattern. Breakdown is seen in the downstream end of the photo. One should note that the streamwise position at which the flow breaks down in the visualisation is farther upstream than for the hot-wire measurements.

Figure 7 shows contours of U_d and u' in a streamwise-spanwise plane at $\eta = 1.55$ for a high-amplitude forcing. The notation high-amplitude forcing corresponds to a maximum initial amplitude of $\approx 7.5\%$ in the fundamental frequency when measured at $x = 210$ mm, whereas forcing at 30% lower speaker voltages is denoted low-amplitude. The spanwise extent of the figure represents $2\lambda_{z,0}$ [1] and the streamwise region covers the distance from the position where the forcing is applied to $x = 1520$ mm. U_d is characterized by narrow elongated regions of positive and negative values with a spanwise wavelength of $\lambda_{z,0}/2$ (see *figure 7(a)*, note that the z-axis is stretched relative to the x-axis). After an initial growth in amplitude, U_d stays almost constant between $x = 400$ mm and $x = 1200$ mm. Starting at $x \approx 1200$ mm both the amplitude and the

[1] The spanwise wave length of the oblique waves is denoted $\lambda_{z,0}$.

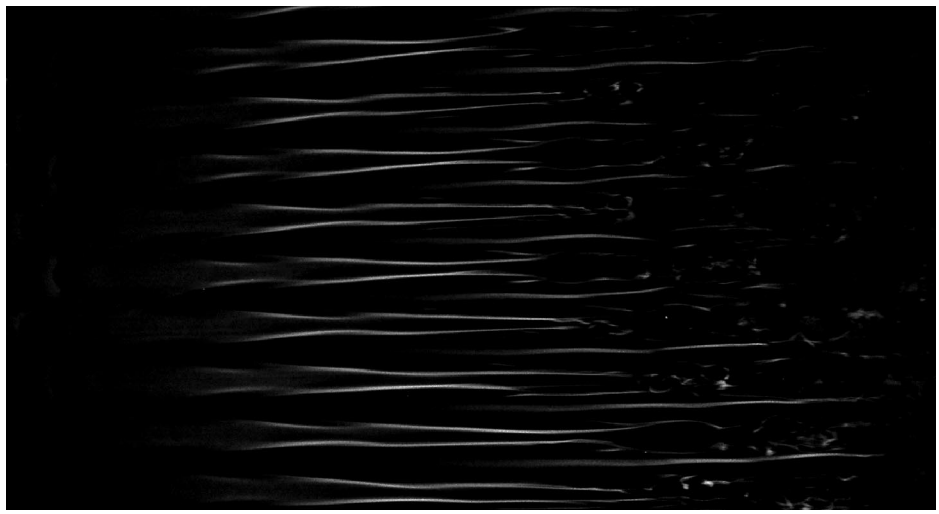

Figure 6. Flow visualisation of oblique transition showing a streamwise-spanwise plane where the flow is from left to right; $U_0 = 7.0$ m/s and $F = 97$.

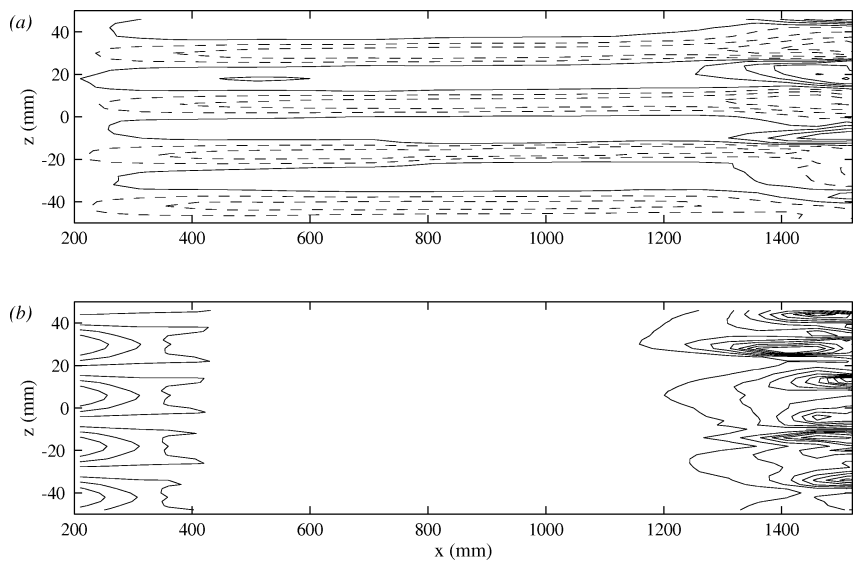

Figure 7. Contour plots in a streamwise-spanwise plane at $\eta = 1.55$ with a high-amplitude forcing for $F = 43$, $U_0 = 9.1$ m/s and $\beta_0 = 131$ m^{-1}. (a) U_d, contours: ±2%, ±6%,…; (b) u', contours: 2%, 4%,….

dominating spanwise wavelength is seen to increase downstream. The wave amplitude u' (see *figure 7(b)*) decays downstream of the disturbance source, and at the same time the spanwise positions of the maxima change from the centre of low-speed streaks to regions between low- and high-speed streaks at $x = 400$ mm. Near $x = 1200$ mm the amplitude starts to grow and downstream of $x \approx 1300$ mm maxima of u' are located at spanwise positions between low- and high-speed regions.

The formation of the streaks and how their spanwise positions relate to the forcing are illustrated by *figure 8*, which shows spanwise profiles of amplitude and phase at the fundamental frequency and also U_d. At $x = 210$ mm, which is about 20 mm downstream of the wave generator, the maximum amplitude of the wave disturbance is approximately 7.5% and the phase changes by 180° at each position where the amplitude

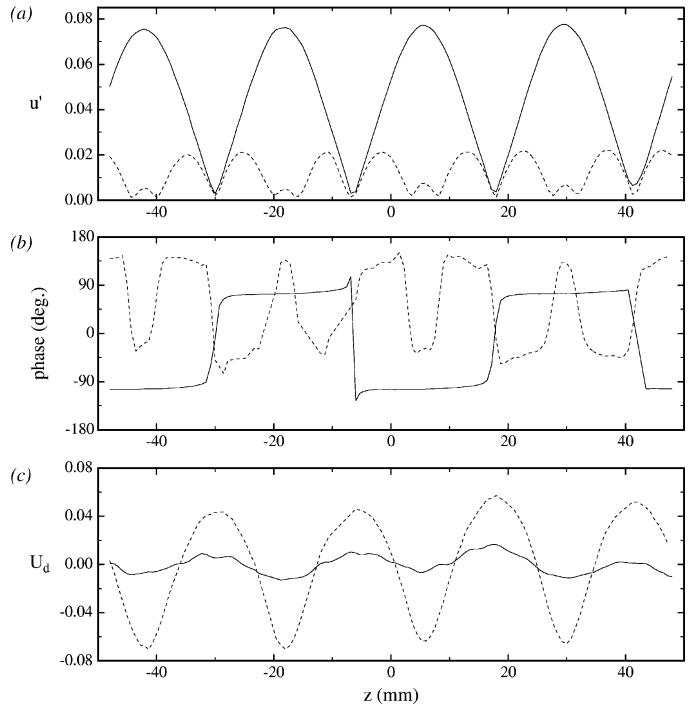

Figure 8. Spanwise profiles at $\eta = 1.55$ of: (a) u'; (b) phase; (c) U_d. ——, measurements at $x = 210$ mm; – – –, $x = 410$ mm. Same conditions as in *figure 7*.

goes to zero. The streaks are not fully developed at this position but a cosine shaped distribution can be observed with minima in U_d at spanwise positions where the wave amplitude attains maxima. However, at the second streamwise position U_d has increased to a value of about $\pm 6\%$ while the wave amplitude has decayed ($u' \approx 2\%$) and changed its structure. Maxima in u' are now connected to spanwise positions located at the zero-crossings of U_d, which is the result of a higher amplitude in the spanwise wavenumber $3\beta_0$ than in the original wavenumber β_0.

Figure 9 shows contours of U_d in cross-stream planes. In order to illustrate the increase of disturbance size with the streamwise direction, the wall-normal coordinate is presented here in dimensional units. For reference, the boundary layer edge ($\eta = 5$) and $\eta = 2$ are indicated by horizontal dotted lines at each streamwise position. A wall normal position of $\eta = 2$ is approximately where the maximum streak amplitude is located and also where so-called Klebanoff modes [2] have their maximum amplitude. When comparing the figures at $x = 410$, $x = 610$ and $x = 1210$ mm (*figure 9(a)–(c)*) the maximum amplitude is observed to be similar, and also the spanwise position of the streaks is constant. It can be observed that the streaks extend across the full boundary layer at all x, i.e. the streaks grow in the wall-normal direction at the same rate as the boundary layer. However, the disturbance does not deform the boundary layer edge significantly in contrast to, e.g., the vortex dominated Görtler flow. This indicates that the cross stream velocity is weak in the present case. [3] At $x = 1610$ mm

[2] Klebanoff modes are, e.g., observed in Blasius flows subjected to elevated levels of free stream turbulence (described in Kendall [39]).

[3] In the experiment by Elofsson and Alfredsson [13] on oblique transition in channel flow, they tried to determine the cross stream velocity related to the streaks, but concluded that it was too small (<1% of the centreline velocity) to be measured with the hot-wire technique employed. In their Appendix they show that the initial interaction of the two waves gives rise to streamwise vorticity responsible for the formation of streaks, however the non-modal growth of streaks does not require streamwise vorticity.

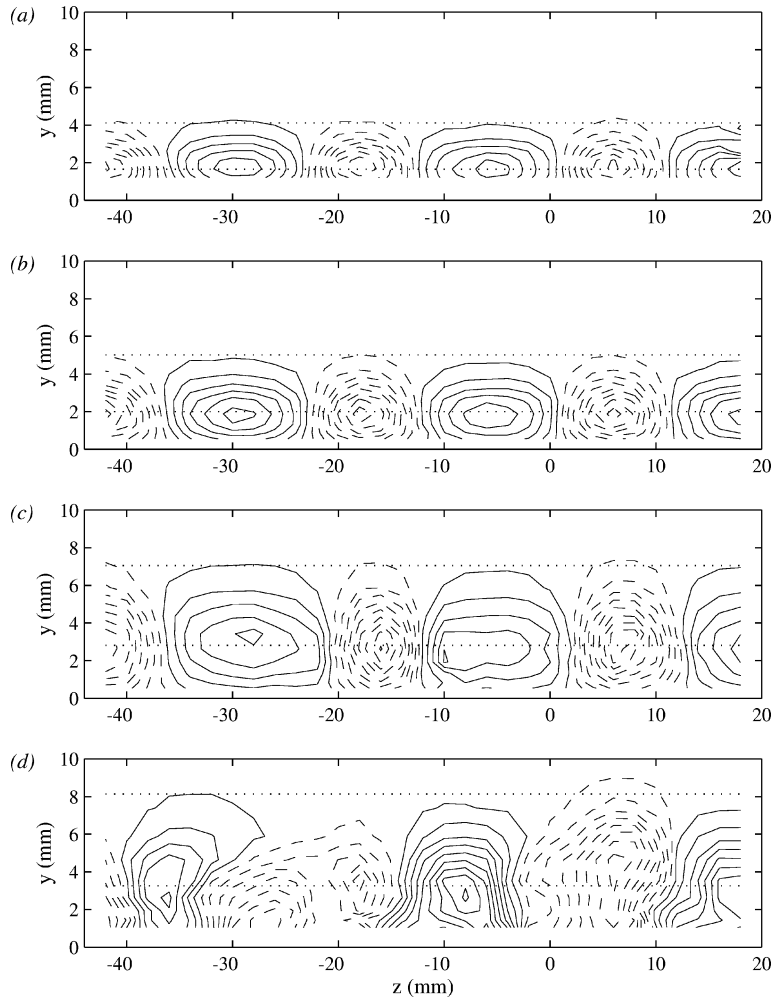

Figure 9. Contour plots of U_d in cross-stream planes for a high-amplitude forcing with $F = 43$, $U_0 = 9.1$ m/s and $\beta_0 = 131$ m^{-1}. (a) Measurements at $x = 410$ mm; (b) $x = 610$ mm; (c) $x = 1210$ mm; (d) $x = 1610$ mm. Contours in (a)–(c): $\pm 0.5\%$, $\pm 1.5\%$,...; in (d): $\pm 1\%$, $\pm 3\%$,....

(*figure 9(d)*) the picture is quite different. Both the streak positions and the spanwise wavelength have now changed and the amplitude has increased from its value at $x = 1210$ mm.

The corresponding contours of u' are shown in *figure 10*. At $x = 410$ mm the structure is dominated by amplitude maxima located at $y \approx 1.5$ mm and at spanwise positions between the streaks. Maxima with a slightly lower amplitude are also observed further out from the wall at spanwise positions where U_d is negative. These maxima grow in amplitude and move closer to the wall at the next measurement station ($x = 610$ mm), whereas the amplitude maxima associated with spanwise gradients in U_d have decayed at this position. *Figure 10(c)* displays contours at $x = 1210$ mm where a larger spanwise wavelength is observed together with an increased peak amplitude. Yet a larger amplitude appears at $x = 1610$ mm where the structure bears some resemblance with the one at the first streamwise position, though extended in the wall-normal direction and slightly shifted along the z-axis. When forcing with a 20% lower amplitude the structure will look in a similar way except for $x = 610$ mm, where only the maxima associated with low-speed regions are visible.

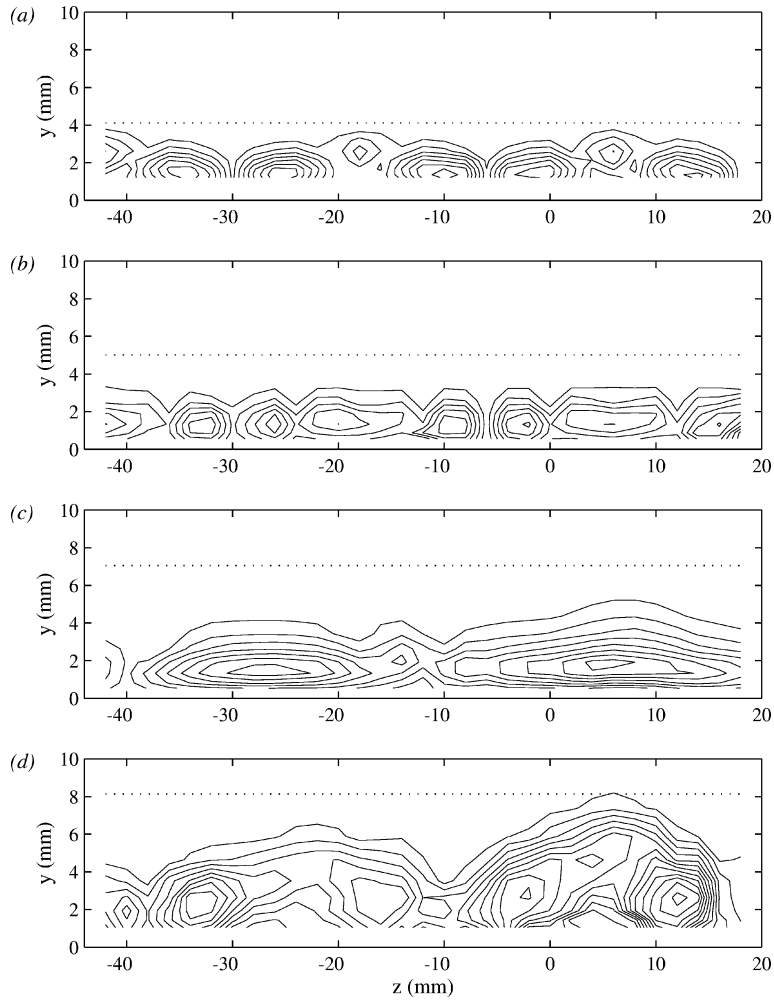

Figure 10. Contour plots of u' in cross-stream planes for same conditions as in figure 9. (a) Measurements at $x = 410$ mm; (b) $x = 610$ mm; (c) $x = 1210$ mm; (d) $x = 1610$ mm. Contours in (a)–(c): 0.2%, 0.4%,...; in (d): 1%, 2%,....

4.2. Spectral representation

Information about the behaviour of individual frequency-wavenumber modes was obtained by applying Fourier transforms to the measured data. The analysis was made with the aid of Matlab scripts. Data sets were multiplied with a Kaiser–Bessel type window before time sequences were Fourier transformed and the resulting amplitudes were corrected for the window functions. The amplitudes were recalculated to correspond to amplitudes in frequency bands of 1 Hz before being plotted. No windowing was used for the spanwise Fourier transform.

Figure 11 shows the streamwise evolution of the amplitude of (ω, β)-modes for two different forcing amplitudes. A frequency-wavenumber decomposition was made at 10 heights through the boundary layer, and for each mode the maximum amplitude was plotted. The data was measured over a distance of one spanwise wavelength of the original wave with a separation of 2 mm between the points. From the two figures it can be seen that the difference in forcing amplitude does not influence the general character. For a higher initial amplitude (*figure 11(b)*), the mode amplitudes are higher and the growth of modes with higher frequencies sets

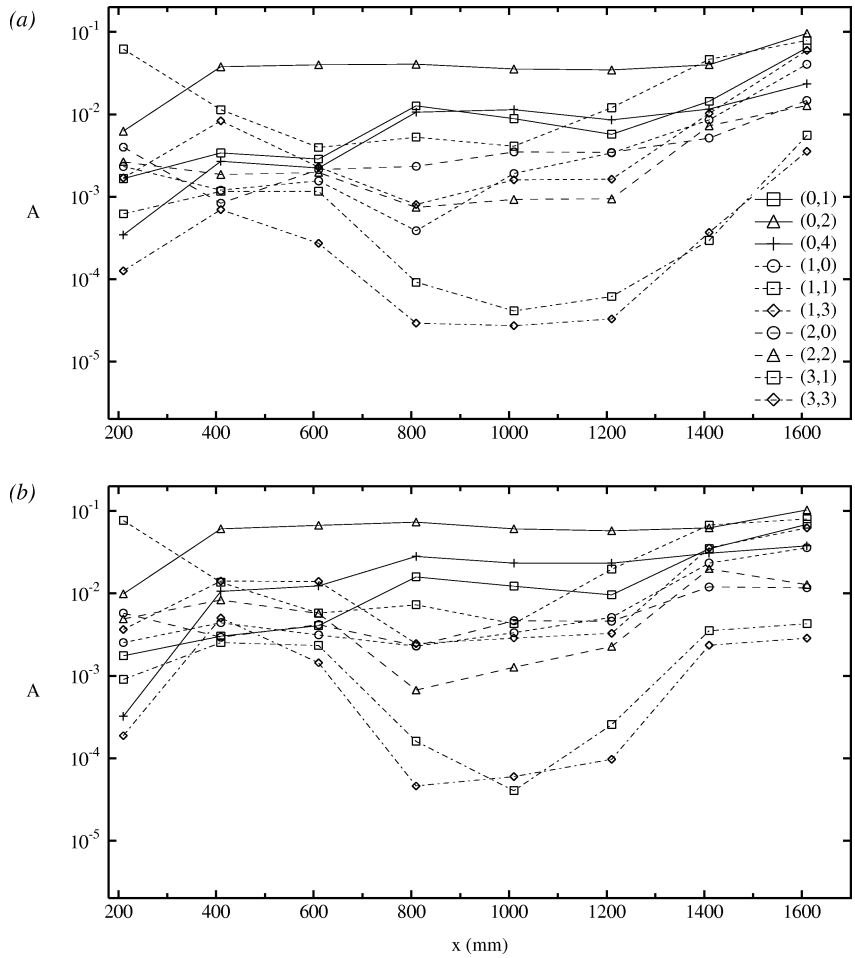

Figure 11. Amplitude of (ω, β)-modes normalized by $U_0 = 9.1$ m/s for different forcing amplitudes with $F = 43$ and $\beta_0 = 131$ m^{-1}. (a) Low-amplitude forcing; (b) high-amplitude forcing.

in at an earlier streamwise position than for the lower initial amplitude (*figure 11(a)*). Initially the modes of highest amplitude are the (1,1) and the (0,2), where the former initially decays and the amplitude of the latter is almost constant after $x = 400$ mm. The initial decay of the (1,1) mode ceases near $x = 600$ mm and the mode starts to grow downstream, which can be understood by comparing with the conditions for zero growth. For a growing boundary layer at the conditions of *figure 11* (for the oblique mode in question $F = 43$ and $\beta_0 = 131$ m^{-1}), branch I is located near $x = 680$ and branch II near $x = 1360$ mm. A strong growth of modes with non-zero frequencies sets in at $x \approx 1200$ mm for the lower initial amplitude and further upstream for the higher. One can also note that the (0,1) mode grows to a large amplitude at the last measurement positions, which was also seen as a change in the streak spacing in *figure 7(a)*. A similar distribution of mode-amplitudes at the first streamwise positions was also obtained from a decomposition of measurements extending over two spanwise wavelengths at a constant boundary layer height of $\eta = 1.55$.

Wall-normal profiles of some of the most important modes are presented in *figure 12* for various streamwise positions. The figures are based on the same data as was used in *figure 11*. During the measurements the main interest was in capturing the streak amplitude and therefore information is lacking in the region closest to the wall. Profiles of the (0,2)-mode have similar shape at all streamwise positions with the maximum located

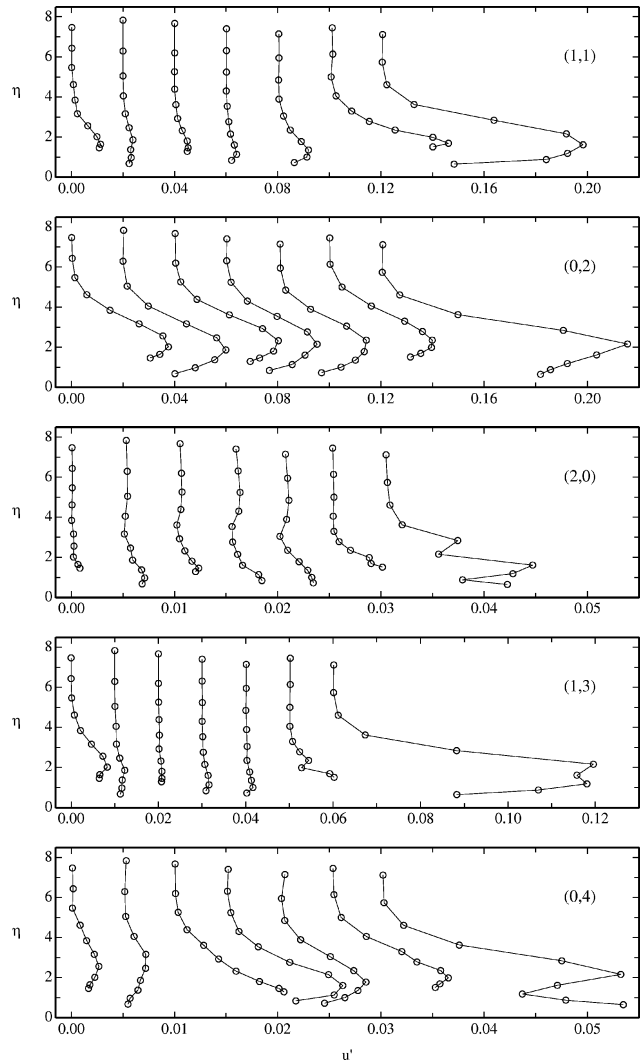

Figure 12. Wall-normal profiles of amplitude in (ω, β)-modes from measurements at $x = 410$, 610, 810, 1010, 1210, 1410 and 1610 mm. Same conditions as in *figure 11(a)*.

near $\eta = 2.2$, while the amplitude maximum of the other stationary mode appears at an increasing height with increasing x (if the two first streamwise positions are excluded).

Figure 13 shows amplitude spectra measured at different streamwise positions for a fixed η and spanwise position. A reference level is indicated to the right of each spectrum. Besides the generated frequency and its harmonics, additional peaks are observed at the first streamwise positions. These elevations above the background level are believed to originate from probe vibrations caused by vortex shedding from the midsection of the boundary layer probe. When proceeding downstream transition is first observed as an increase in the amplitude of harmonics, later followed by a distributed elevation of the amplitude at all frequencies. One can note the rapid increase in the amplitude of higher frequencies occurring between $x = 1360$ and $x = 1510$ mm, a distance of approximately two streamwise wavelengths of the initial oblique waves. Spectra measured at $z = 24.7$ mm (not shown) had a narrower range of frequencies that were elevated above the background level.

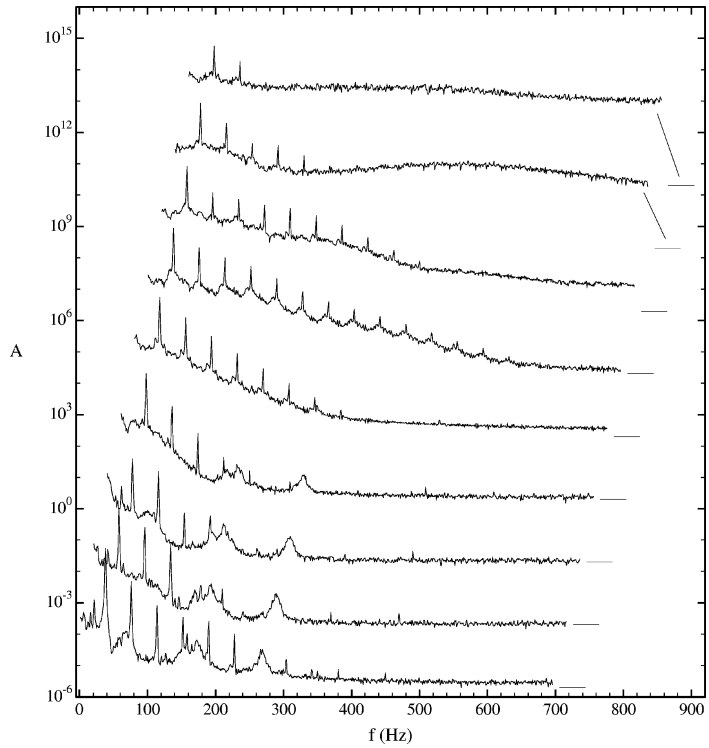

Figure 13. Amplitude spectra for a low-amplitude forcing at $U_0 = 9.1$ m/s and $F = 43$. Measurements at $\eta = 1.5$, $z = 29.2$ mm and $x = 210$, 610, 1010, 1210, 1310, 1360, 1410, 1460 and 1510 mm. Consecutive spectra are shifted 20 Hz and multiplied by 10^{2n}.

For this case the rapid growth started a bit further downstream than for the spanwise position shown in *figure 13*, however, spectra measured at the two most downstream positions were similar for both cases.

4.3. Time representation

Phase-averaged velocity data from streamwise positions near the disturbance generator are shown in *figure 14*. Each figure shows contours of u over three periods in time from a region covering two spanwise wavelengths of the oblique waves. The data is the average of 25 sets of triggered velocity traces measured at 129 equidistant spanwise positions. Since the horizontal axes display the time, a spatial representation of the fields is obtained by assuming that the flow is from right to left. The first figure shows the field at $x = 210$ mm where a regular wave pattern is seen. Further downstream Λ-shaped regions of positive or negative deviations from the time average are observed in a staggered pattern. At the streamwise positions shown in this figure, the amplitude of the time dependent disturbances decays (as the stationary streaks increase in amplitude).

Characteristic velocity traces from three streamwise positions are shown in *figure 15* for 6 periods of the initial waves. The traces are grouped after which height in the boundary layer they were measured at, and the traces within each group represents from bottom to top $x = 1410$, 1510 and 1610 mm. All traces were measured for a high-amplitude forcing at $z = -12$ mm, which corresponds to a position between a low- and high-speed streak. At $\eta = 1.4$ and $x = 1510$ mm a high-frequency motion of low amplitude is seen over a few periods and at the last streamwise position the amplitude of higher frequencies have increased substantially and can now be observed at all three wall-normal positions. At $\eta = 2.7$, $x = 1610$ mm the signal indicates the presence of

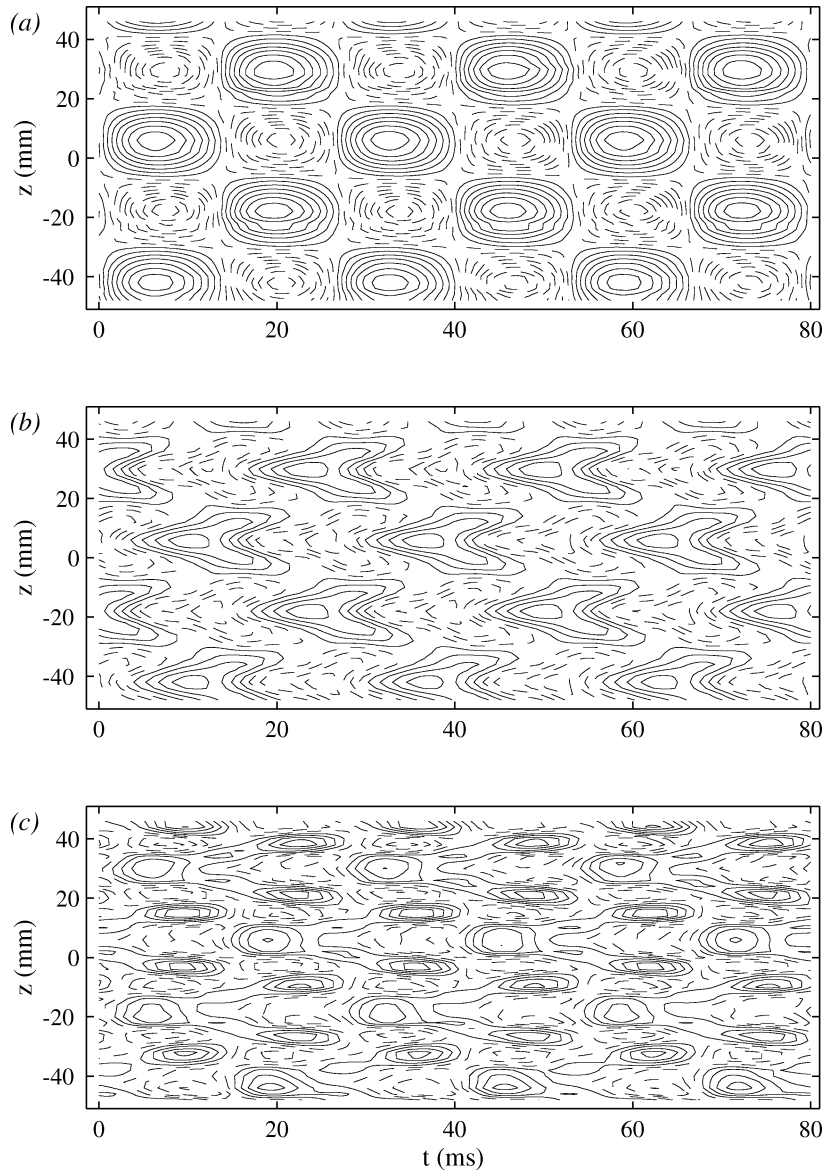

Figure 14. Contours of u at $\eta = 1.5$ for a high-amplitude forcing with $F = 43$ and $\beta_0 = 131\ \mathrm{m}^{-1}$ at $U_0 = 9.1$ m/s. (a) Measurements at $x = 210$; (b) $x = 310$; (c) $x = 610$ mm. Contour spacing is 1% in (a),(b) and 0.5% in (c).

so called ‘spikes’. Spikes are normally seen at the peak-position, however because of lack of data we cannot confirm that such spikes also occur there for the present case.

5. Summary and discussion

Results from an experimental investigation of oblique transition in a Blasius boundary layer have been reported, where wave disturbances were generated with periodic blowing and suction through a spanwise array of pipes. The disturbance generating system was found to give waves which develop in agreement with linear theory.

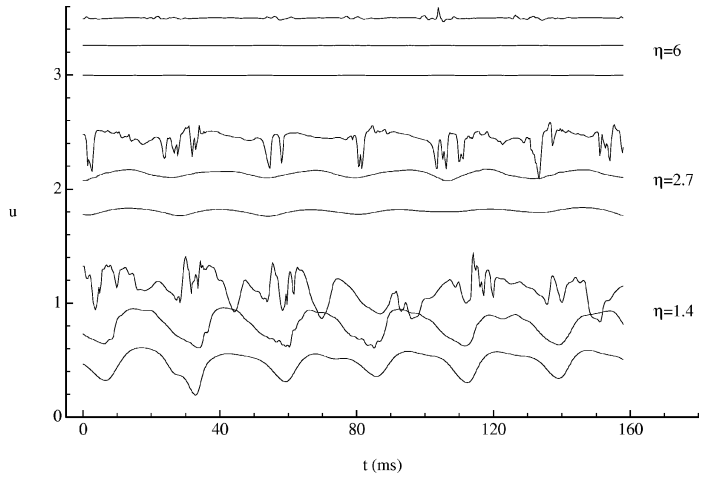

Figure 15. Velocity traces at $z = -12$ mm and $x = 1410$, 1510 and 1610 mm are shown at three heights through the boundary layer. Traces at each height are separated by 0.3 U_0 and represents, from bottom to top, $x = 1410$, 1510 and 1610 mm.

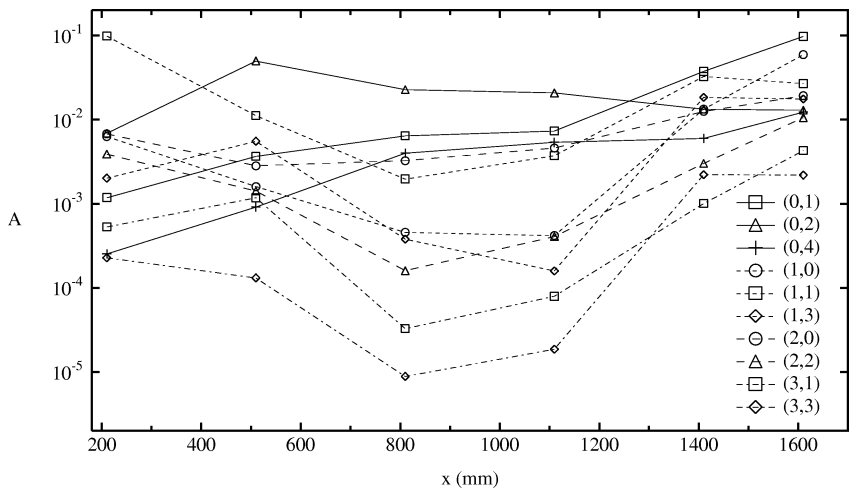

Figure 16. Amplitude of (ω, β)-modes normalized by $U_0 = 9.1$ m/s for a high-amplitude forcing with $F = 43$ and $\beta_0 = 163$ m^{-1}.

The forcing of two oblique waves resulted in an interaction and the formation of streamwise streaks. The streaks were found to grow initially until they saturate and then their amplitude stays nearly constant over a streamwise distance of about 800 mm. When viewed in cross-stream planes, the streaks were seen to be located inside the boundary layer with their maximum amplitude at a wall-normal position near $\eta = 2$.

The breakdown of the streaks occurs through the growth of higher harmonics of the initial waves and from a decomposition of the disturbance amplitude into individual frequency-wavenumber modes, the streamwise evolution of the amplitude in (ω, β) modes could be followed. The decomposition also allowed wall-normal profiles to be plotted. Other features seen in the transition process was the appearance at upstream positions of Λ-shaped structures in a staggered pattern, which is similar to subharmonic or N-breakdown (see the discussion in [15]).

Results from flow visualizations, where a smoke-layer was introduced near the flat plate surface, showed oblique waves which interact to give streaky structures, followed by elongated Λ-structures and finally

breakdown. Structures with a short streamwise wavelength were observed on the sides of the low-speed regions prior to breakdown.

From studies on optimal transient growth it is known that the largest growth occurs for a specific value of the spanwise wavenumber β. We investigated two different spanwise wavelengths and *figure 16* shows the amplitude growth for a smaller wavelength (a higher value of β) than in *figure 11*. The major difference compared with the smaller β is that starting from $x \approx 1200$ mm the dominating stationary disturbance is now the (0,1)-mode instead of the (0,2). This can probably be explained by comparing with the β that gives the largest transient growth. Butler and Farrell [25] found the optimal spanwise wavelength to be $\beta\delta^* = 0.65$ at $Re_{\delta^*} = 1000$ for a parallel Blasius flow, where $\delta^* = 1.72(\nu x/U_0)^{1/2}$. This can be compared with the experimental values of the fundamental spanwise wavenumber which are $\beta\delta^* = 0.37$ for the standard spacing and $\beta\delta^* = 0.46$ for the narrow spacing at $x = 1610$. The corresponding values for the (0,2) mode are twice as large and at the last streamwise position for the narrow case, β for (0,1) is closer to the optimal spanwise wavenumber than (0,2). However, according to the investigation by Andersson et al. [30] on spatial optimal disturbances in a growing boundary layer, the optimal β would rather be $\beta\delta = 0.45$ or $\beta\delta^* = 0.77$. Their calculations determined the disturbance at the leading edge which experienced the largest spatial energy growth when observed at a downstream position x.

In the present investigation of oblique transition, a general picture of the transition scenario can be described as follows: a rapid growth of streamwise streaks together with a decay in the amplitude of the initial oblique waves, a second stage where the streak amplitude is constant and a growth of the oblique waves which might be governed by linear stability, followed by the final stage where both stationary and time-dependent modes grow, eventually evolving into a turbulent state.

The amplitude of the streaks in the first stage depends on the wave amplitude, the decay rate of the oblique waves, the spanwise wavenumber and the Reynolds number at the disturbance source. The non-modal growth is governed by the latter two, whereas the first two determine the input to the streamwise vortices through a nonlinear interaction. For the conditions presented in this report a streak amplitude (ΔU) of $\approx \pm 5\%$ of U_0 was reached near $x = 800$ mm. From measurements at a higher F, where the initial decay of the oblique waves is smaller, a streak amplitude of about $\pm 13\%$ of U_0 was reached (see also *table II*). Despite the larger streak amplitude in this case, the location for the transition onset did move upstream with less than 100 mm. The growth of the waves in the second stage is motivated by the observations made in connection with *figure 11*, where it was found that the growth of the (1,1) mode started at the location of branch I for the present conditions. In the final stage, the mode which has the highest amplitude will depend on the specific conditions. In particular, the effect of the initial amplitude and the spanwise wavenumber was shown in section 4.2.

Berlin et al. [15] reported on measurements and direct numerical simulations at $U_0 = 12$ m/s and $F = 59$. The measurements indicated the appearance of high-frequency fluctuations approximately 350 mm downstream of the disturbance source. A similar development could be obtained in the direct numerical simulations by a detailed modelling of the disturbance source. The growth observed in the DNS was quite sensitive to the

Table II. Experimental conditions and results for some of the investigated cases. u'_0 is the maximum amplitude of the two oblique waves at $x = 210$ mm. u'_0 and ΔU are given as percent of U_0.

U_0	F	β	u'_0	$\Delta U(x = 1000$ mm)
9.1 m/s	43	131 m^{-1}	8.5%	$\pm 5\%$
9.1 m/s	43	131 m^{-1}	6.3%	$\pm 3.5\%$
9.1 m/s	43	163 m^{-1}	9.5%	$\pm 2.5\%$
8.2 m/s	59	131 m^{-1}	9.0%	$\pm 13\%$

method used for modelling the disturbances and the method which was finally chosen resulted in the most rapid development. It can be hypothesized that the forcing method used in the present experiments, where disturbances from individual pipes are mixed in a common slit before entering the boundary layer, results in a different transition location than for the wave generator used in the measurements reported by Berlin et al. They used separate slits for each spanwise position and the edge effects of these slits may result in disturbance energy also in smaller spanwise scales. However, the main reason for the difference with the present investigation is probably the conditions that determine the non-modal growth of the streaks, and thereby the conditions for streak instability.

In an experimental investigation of oblique transition in plane Poiseuille flow at a subcritical Reynolds number (Elofsson and Alfredsson [13]), transition only occurred if the streak amplitude reached above a threshold level. For the present study in a Blasius flow, there is a second chance for transition to occur even if the streak amplitude at the initial stage is not sufficiently high to directly trigger a streak instability. Initially the generated oblique waves are damped, but as the wave travels downstream it reaches the unstable region and starts to grow, whereafter the final stage shows a strong growth of both stationary and time-dependent modes.

Finally we would like to point out that although the oblique transition scenario is of interest by itself, it has relevance also for other types of transition scenarios. First of all it is an excellent way to introduce well defined streaky structures into the flow, which subsequently grow and break down. Streak growth and breakdown are known to occur for transition under elevated levels of free stream turbulence. Oblique wave interaction may also occur when wave packets (Gaster-type) interact and this could possibly give rise to similar streaky structures. It is interesting to note that in the standard scenarios (K- and N-breakdown) the importance of the 2D wave is mainly to provide the breeding ground for the oblique waves, whereas the latter dominate the breakdown process.

Acknowledgments

The authors would like to thank Professor H.H. Fernholz for arranging a three month research visit to the Hermann Föttinger Institut at TU-Berlin for PAE in the fall of 1995. The original design of the disturbance source greatly benefited from discussions with Sebastian Bake and Professor Y.S. Kachanov during this visit. The flow visualisations were made in co-operation with Dr. Masaharu Matsubara. Dr. Ardeshir Hanifi kindly provided results from his PSE-calculations. Thanks are also due to Markus Gällstedt for help with manufacturing parts for the experimental setup. This work was supported by the Swedish Research Council for Engineering Sciences (TFR).

References

[1] Klebanoff P.S., Tidstrom K.D., Sargent L.M., The three-dimensional nature of boundary layer instability, J. Fluid Mech. 12 (1962) 1–34.
[2] Kachanov Y.S., Kozlov V.V., Levchenko V.Y., Occurence of Tollmien–Schlichting waves in the boundary layer under the effect of external perturbations, Fluid Dyn. 13 (4) (1979) 704–711 (original, in Russian in: Izv. Akad. Nauk SSSR, Mekh. Zhid. Gaza 5 (1978) 85–94).
[3] Corke T.C., Mangano R.A., Resonant growth of three-dimensional modes in transitional Blasius boundary layers, J. Fluid Mech. 209 (1989) 93–150.
[4] Orszag S.A., Patera A.T., Secondary instability of wall-bounded shear flows, J. Fluid Mech. 128 (1983) 347–385.
[5] Herbert T., Secondary instability of plane channel flow to subharmonic three-dimensional disturbances, Phys. Fluids 26 (1983) 871–874.
[6] Herbert T., Secondary instability of boundary layers, Annu. Rev. Fluid Mech. 20 (1988) 487–526.
[7] Kachanov Yu.S., Physical mechanisms of laminar-boundary-layer transition, Annu. Rev. Fluid Mech. 26 (1994) 411–482.
[8] Kleiser L., Zang T.A., Numerical simulation of transition in wall-bounded shear flows, Annu. Rev. Fluid Mech. 23 (1991) 495–537.
[9] Schmid P.J., Henningson D.S., A new mechanism for rapid transition involving a pair of oblique waves, Phys. Fluids A 4 (1992) 1986–1989.
[10] Joslin R.D., Streett C.L., Chang C.L., Spatial direct numerical simulations of boundary-layer transition mechanisms: Validation of PSE theory, Theor. Comput. Fluid Dyn. 4 (1993) 271–288.

[11] Berlin S., Lundbladh A., Henningson D.S., Spatial simulations of oblique transition in a boundary layer, Phys. Fluids 6 (1994) 1949–1951.
[12] Elofsson P.A., Alfredsson P.H., Experiments on nonlinear interaction between oblique Tollmien–Schlichting waves, in: Kobayashi R. (Ed.), Laminar-Turbulent Transition, Proc. IUTAM Symposium, Sendai, Springer-Verlag, Berlin, 1995, pp. 465–472.
[13] Elofsson P.A., Alfredsson P.H., An experimental study of oblique transition in plane Poiseuille flow, J. Fluid Mech. 358 (1998) 177–202.
[14] Wiegel M., Experimentelle Untersuchung von kontrolliert angeregten dreidimensionalen Wellen in einer Blasius-Grenzschicht, Ph.D. thesis, TH Hannover, 1996.
[15] Berlin S., Wiegel M., Henningson D.S., Numerical and experimental investigations of oblique boundary layer transition, J. Fluid Mech. 393 (1999) 23–57.
[16] Fasel H., Thumm A., Bestek H., Direct numerical simulation of transition in supersonic boundary layers: Oblique breakdown, in: Kral L.D., Zang T.A. (Eds.), Transitional and turbulent compressible flows, ASME FED, Vol. 151, 1993, pp. 77–92.
[17] Chang C.-L., Malik M.R., Oblique-mode breakdown and secondary instability in supersonic boundary layers, J. Fluid Mech. 273 (1994) 323–360.
[18] Gathmann R.J., Si-Ameur M., Mathey F., Numerical simulations of three-dimensional natural transition in the compressible confined shear layer, Phys. Fluids A 5 (1993) 2946–2968.
[19] Sandham N.D., Adams N.A., Kleiser L., Direct simulation of breakdown to turbulence following oblique instability waves in a supersonic boundary layer, in: Voke P.R., Kleiser L., Chollet J.P. (Eds.), Direct and Large-Eddy Simulation I, Kluwer, 1994, pp. 213–223.
[20] Ellingsen T., Palm E., Stability of linear flow, Phys. Fluids 18 (1975) 487–488.
[21] Landahl M.T., A note on an algebraic instability of inviscid parallel shear flows, J. Fluid Mech. 98 (1980) 243–251.
[22] Hultgren L.S., Gustavsson L.H., Algebraic growth of disturbances in a laminar boundary layer, Phys. Fluids 24 (1981) 1000–1004.
[23] Boberg L., Brosa U., Onset of turbulence in a pipe, Z. Naturforsch. 43 (1988) 697–726.
[24] Gustavsson L.H., Energy growth of three-dimensional disturbances in plane Poiseuille flow, J. Fluid Mech. 224 (1991) 241–260.
[25] Butler K.M., Farrell B.F., Three-dimensional optimal perturbations in viscous shear flow, Phys. Fluids A 4 (1992) 1637–1650.
[26] Klingmann B.G.B., On transition due to three-dimensional disturbances in plane Poiseuille flow, J. Fluid Mech. 240 (1992) 167–195.
[27] Trefethen L.N., Trefethen A.E., Reddy S.C., Driscoll T.A., Hydrodynamic stability without eigenvalues, Science 261 (1993) 578–584.
[28] Henningson D.S., Bypass transition and linear growth mechanisms, in: Benzi R. (Ed.), Advances in Turbulence V, Kluwer, Dordrecht, 1995, pp. 190–204.
[29] Luchini P., Reynolds-number-independent instability of the boundary layer over a flat surface. Optimal perturbations, J. Fluid Mech. 404 (2000) 289–309.
[30] Andersson P., Berggren M., Henningson D.S., Optimal disturbances and bypass transition in boundary layers, Phys. Fluids 11 (1999) 134–150.
[31] Reddy S.C., Schmid P.J., Baggett J.S., Henningson D.S., On stability of streamwise streaks and transition thresholds in plane channel flows, J. Fluid Mech. 365 (1998) 269–303.
[32] Elofsson P.A., Kawakami M., Alfredsson P.H., Experiments on the stability of streamwise streaks in plane Poiseuille flow, Phys. Fluids 11 (1999) 915–930.
[33] Waleffe F., Hydrodynamic stability and turbulence: Beyond transients to a self-sustaining process, Stud. Appl. Math. 95 (1995) 319–343.
[34] Waleffe F., On a self-sustaining process in shear flows, Phys. Fluids 9 (1997) 883–900.
[35] Bakchinov A.A., Grek G.R., Klingmann B.G.B., Kozlov V.V., Transition experiments in a boundary layer with embedded streamwise vortices, Phys. Fluids 7 (1995) 820–832.
[36] Johansson A.V., A low speed wind-tunnel with extreme flow quality – design and tests, in: Proc. 18th ICAS Congress, Beijing, Sept. 1992, pp. 1603–1611.
[37] Bake S., Kachanov Y.S., Fernholz H.H., Subharmonic K-regime of boundary-layer breakdown, in: Henkes R.A.W.M., van Ingen J.L. (Eds.), Proc. Transitional Boundary Layers in Aeronautics, Royal Netherlands Academy of Arts and Sciences, Elsevier Science Publishers, 1996, pp. 81–88.
[38] Gaponenko V.R., Kachanov Y.S., New methods of generation of controlled spectrum instability waves in the boundary layers, in: International Conference on Methods of Aerophysical Research. Part 1, 1994, Novosibirsk, ITAM, pp. 90–97.
[39] Kendall J.M., Experimental study of disturbances produced in a pre-transitional laminar boundary layer by weak freestream turbulence, AIAA Paper 85-1695 (1985).